Migration of atmospheric convection coupled with ocean currents pushes El Niño to extremes

WonMoo Kim[1,2], Wenju Cai[1], and Jong-Seong Kug[3]

[1]CSIRO Marine and Atmospheric Research, Melbourne, Victoria, Australia, [2]Center for Climate/Environment Change Prediction Research, Ewha Womans University, Seoul, South Korea, [3]School of Environmental Science and Engineering, Pohang University of Science and Technology, Pohang, South Korea

Abstract The warm phase of El Niño–Southern Oscillation can grow much stronger than the cold phase, but the associated dynamics are not well understood. Here we show that the anomalous zonal advection of warm water is the major process that pushes El Niño to extremes and that this anomalous advection results from the coupling of oceanic currents with eastward migration of the atmospheric convection; a greater zonal advection is associated with a greater extent of the eastward migration. By contrast, there is a limited extent for westward migration during La Niña. Climate models that successfully simulate the amplitude asymmetry display a systematic linkage of a greater longitudinal movement of the convection center with a stronger zonal advection and greater El Niño amplitude. In a warming world, the longitudinal migration of convection response increases, as does the role of zonal advection, increasing the frequency of future extremes of El Niño.

1. Introduction

El Niño–Southern Oscillation (ENSO) is a dominant mode of natural climate variability spurring global-scale weather-related disasters [*Kerr*, 1999]. The location, intensity, and scale of impact differ greatly according to its phase, namely, El Niño (warm) and La Niña (cool) [*Cai et al.*, 2010; *Frauen et al.*, 2014; *Hoerling et al.*, 1997]. The amplitude of El Niño can grow far greater than that of the La Niña counterpart [*An and Jin*, 2004], with a commensurately different impact. Understanding the cause of this amplitude asymmetry, in general, and the mechanism of extreme El Niño events in particular, has been a long-standing issue [*An and Jin*, 2004; *Duan et al.*, 2008; *Frauen and Dommenget*, 2010; *Monahan and Dai*, 2004; *Su et al.*, 2010; *Yeo and Kim*, 2014]. During the boreal winters of 1982–1983 and 1997–1998, the area-averaged sea surface temperature anomaly (SSTa) over the Niño3 region (150°W–90°W, 5°S–5°N) reached up to +3°C and many parts of the world experienced exceptional weather extremes such as catastrophic floods, severe droughts, and devastating hurricanes [*McPhaden*, 1999; *Philander*, 1983]. The extreme El Niño event of 1997–1998 alone caused an estimated loss of $50 billion and 23,000 fatalities worldwide [*Sponberg*, 1999]. On the other hand, a negative SSTa has rarely reached amplitude of even −2°C over the 20th century (Figure 1a).

Several mechanisms have been suggested for this asymmetric behavior of ENSO. These include the role of nonlinear vertical advection on El Niño-La Niña asymmetry [*An and Jin*, 2004; *Jin et al.*, 2003], which pointed out that when El Niño anomaly propagates eastward from the subsurface, the anomalously warm water is upwelled and intensifies the existing anomaly. Some studies argue that the horizontal advection enhances ENSO asymmetry during the developing stage, while vertical advection comes into action after the mature stage [*Kim and Cai*, 2014; *Su et al.*, 2010]. Others highlighted the role of the nonlinear SST-wind feedback [*Frauen and Dommenget*, 2010; *Philip and van Oldenborgh*, 2009], biological feedback [*Park et al.*, 2011], fundamental nonlinearity of the system [*Timmermann et al.*, 2003], or stochastic forcing including westerly wind bursts [*Gebbie et al.*, 2007], but there is no consensus, and this issue of what drives an El Niño into extreme continues to challenge scientist worldwide. Here we provide a new mechanism that highlights that the linear zonal advection and the migration of atmospheric convection coupled with ocean currents are the major processes that push El Niño to extremes.

2. Data and Methods

2.1. Data

Extended Reconstructed Sea Surface Temperature version 3b (ERSSTv3b) [*Smith et al.*, 2008] is used to calculate the observed skewness. Simple Ocean Data Assimilation version 2.2.4 (SODA2.2.4) [*Carton and Giese*, 2008]
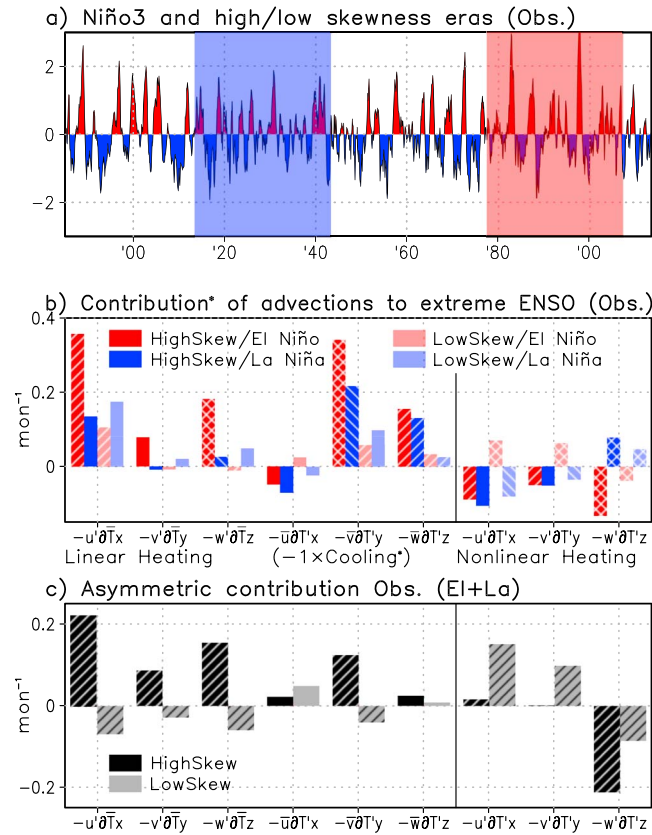
Figure 1. Observational reanalysis. (a) Niño3 SSTa index. High and low skewness eras are indicated by red and blue colors, respectively. (b) Contribution of advections to extreme ENSO development. Dark (light) red bars represent the average contributions to El Niño peaks during the high (low) skewness era, while blue bars are for La Niña peaks. Contributions to La Niña peaks are multiplied by −1 for direct comparison. (c) Asymmetric contributions (sum of El Niño and La Niña) in the observation. Positive value means net positive contribution, i.e., stronger El Niño/weaker La Niña. Dark and light grey bars indicate high and low skewness era, respectively. Significant differences at the 95% confidence level (Student's *t* test) between the high and the low skewness eras (El Niño and La Niña) are indicated by top-right–bottom-left (top-left–bottom-right in Figure 1b only) diagonal lines.

is also utilized to estimate the heat budget and wind-stress forcing. The analysis period for the observations is from 1900 to 2013 (2010 for SODA2.2.4). Here we loosely refer to the observational reanalysis products as the observation for the brevity. Rainfall variability is estimated from the Global Precipitation Climatology Project (GPCP) [*Adler et al.*, 2003] data for the recent period (1979–2013). For climate model simulations, historical runs (r1i1p1) of 22 Coupled Model Intercomparison Project Phase 5 (CMIP5; Table S1 in the supporting information) model simulations that cover from 1885 to 2005 are used, while the future state is assessed for Representative Concentration Pathways scenario 8.5 (RCP8.5) [*Taylor et al.*, 2011] experiment from 2006 to 2100. The list of models is given in Figure 1a (Dark and light amber colors indicate models that are selected as "good" and "less-skewed" models, respectively, which are described in the following section). All model outputs are monthly and preprocessed by linearly interpolating onto a 1°×1° regular grid.

2.2. Measure of Skewness

To estimate and compare ENSO asymmetry between the observations and variety of climate models, we calculated normalized skewness [*An and Jin*, 2004] of area-averaged Niño3 SSTa index of a 31 year running window in the observational reanalysis (1900–2013) and historical simulations (1885–2005) of 22 CMIP5 models (cf. Figure 2a). This calculation is accomplished by first removing 31 year running monthly climatology (m) from the area-averaged SSTa. The skewness (m_3) of SSTa index within the given window is then scaled by its variance (m_2) to give normalized skewness (s) as $s = m_3/m_2^{3/2}$, where m_n is the nth moment about its mean, i.e., $m_n = \sum (x_i - m)^n/N$.
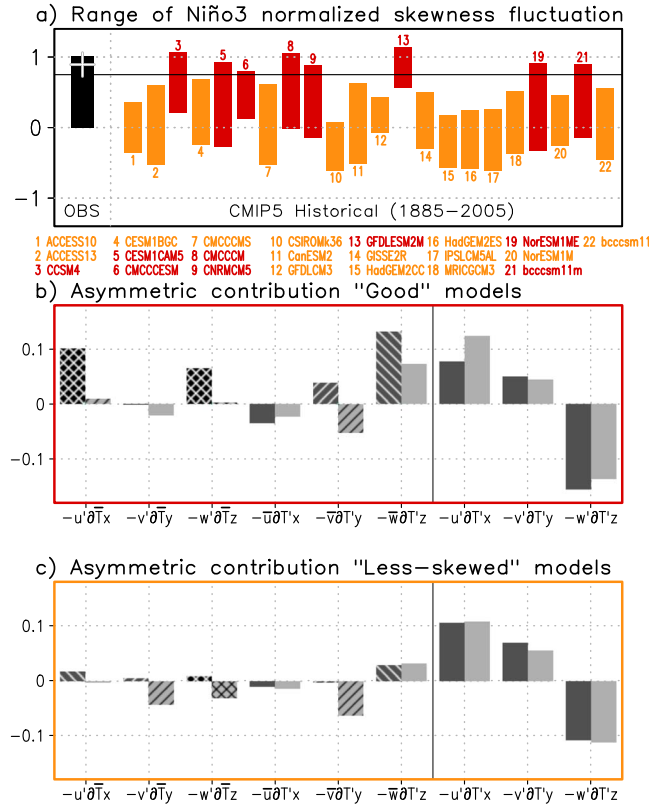
2.3. High/Low Skewness Eras

High and low skewness eras are identified when the normalized skewness of a 31 year window reaches maximum and minimum values in the historical run (Figures S1–S2 in the supporting information), respectively. The maximum and minimum values of normalized skewness are sought within 1900–2013 (whose center years of 31 year window are within 1915–1998) for the observational reanalysis (ERSSTv3b), 1885–2005 (center within 1900–1990) for historical runs, and 2006–2100 (center within 2021–2085) for RCP8.5 runs of CMIP5 models. The two 31 year time slots are referred to as high and low skewness eras, respectively.

Figure 2. Model results. (a) The range of normalized skewness of Niño3 index for ERSSTv3b and 22 CMIP5 historical runs. Current value of normalized skewness is indicated by "plus" sign in the observation. The solid horizontal line indicates the skewness criterion of 0.75, which is used to classify models as good (dark) or less-skewed (light), for the further analysis. (b and c) Same as Figure 1c but for CMIP5 models. Significant differences at the 95% confidence level (Student's t test) between the high and the low skewness eras (good and less-skewed models) are indicated by top-right–bottom-left (top-left–bottom-right) diagonal lines.
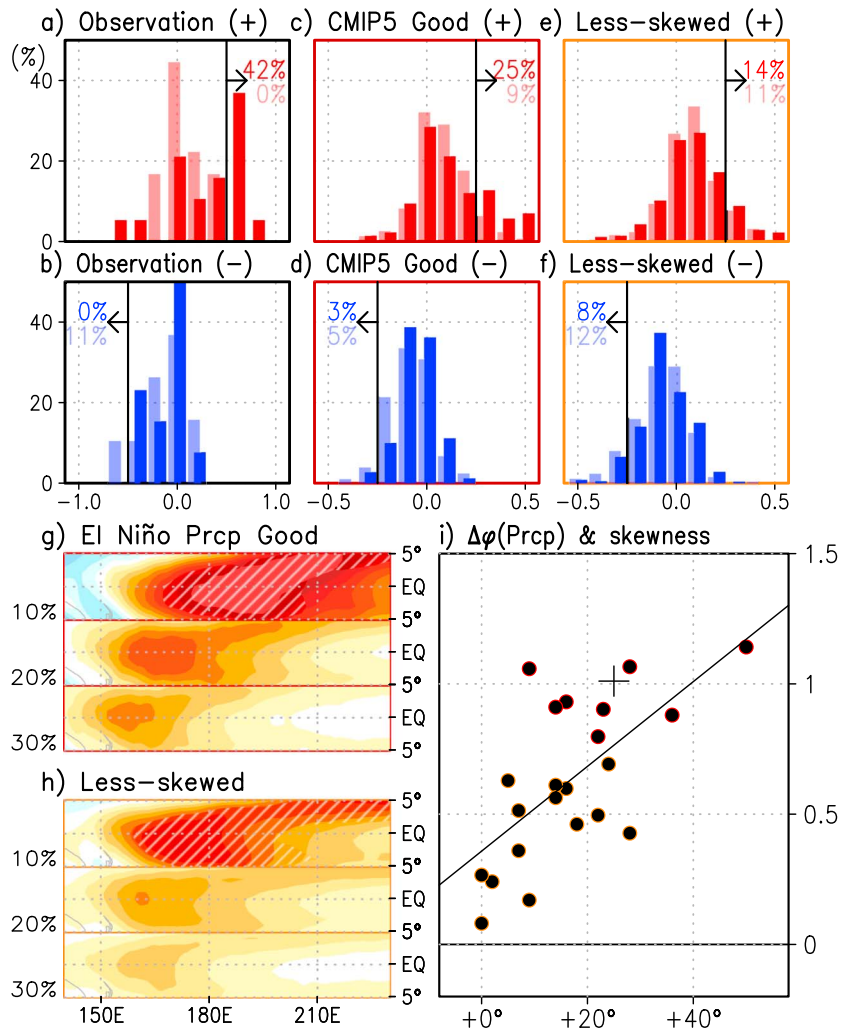
2.4. Selection of Models

To examine what makes some models able to simulate current observed skewness range while others do not, we classified eight good models whose maximum normalized skewness value exceeds +0.75 (i.e., approximately three fourths of observed maximum) during the historical run and the rest as less-skewed models.

2.5. Definition of ENSO Pitch

To target the final push that enhances extreme ENSO, we defined El Niño (La Niña) pitch by following two steps: First, we select extreme ENSO when Niño3 SSTa index is greater than the top (less than the bottom) 10% within the 31 year window. Here we utilized rank statistics, as the characteristics of Niño3 index in models are different, but the main results are unaffected if one uses standard deviations as the criteria. Second, we find the period that is still warming (cooling), i.e., $\partial \text{Niño3}/\partial t \geq 0$ ($\partial \text{Niño3}/\partial t \leq 0$), among the selected events, i.e., the growth phases of these extreme events (Figure S3 in the supporting information).

2.6. Heat Budget

The heat budgets are calculated over the Niño3 region and the top 50 m. The advective heating terms ($-\vec{U} \cdot \nabla T$, where $\vec{U}$ is three-dimensional oceanic current and T is oceanic temperature) are calculated in respect to the 31 year window climatology at each grid point and averaged within the box (cf. Figure S4 in the supporting information). To compare between different model simulations and the observations, each term is scaled by the models' standard deviation of Niño3 SSTa, giving the unit of mon^{-1}. The three terms in each blanket represent the advection of mean temperature by anomalous (zonal, meridional, and vertical) currents, the advection of anomalous temperature by mean currents, and the nonlinear advection, respectively.

$$\frac{1}{\sigma(\text{Niño3})} \frac{\partial T'}{\partial t}\bigg|_{adv} = \frac{1}{\sigma(\text{Niño3})} \left(-\vec{U}' \cdot \nabla \overline{T} - \overline{\vec{U}} \cdot \nabla T' - \vec{U}' \cdot \nabla T' \right)$$

$$= \frac{1}{\sigma(\text{Niño3})} \begin{bmatrix} \left(-u' \cdot \frac{\partial \overline{T}}{\partial x} - v' \cdot \frac{\partial \overline{T}}{\partial y} - w' \cdot \frac{\partial \overline{T}}{\partial z} \right) \\ + \left(-\overline{u} \cdot \frac{\partial T'}{\partial x} - \overline{v} \cdot \frac{\partial T'}{\partial y} - \overline{w} \cdot \frac{\partial T'}{\partial z} \right) \\ + \left(-u' \cdot \frac{\partial T'}{\partial x} - v' \cdot \frac{\partial T'}{\partial y} - w' \cdot \frac{\partial T'}{\partial z} \right) \end{bmatrix}$$

The contribution of each advective heating term is averaged for the ENSO pitches (e.g., Figure 1b). The contributions to La Niña development are multiplied by −1 so that one can directly compare with those to

Figure 3. Zonal advection and convective response. Histogram of the zonal advection for (a and b) observation, (c and d) good models, and (e and f) less-skewed models, respectively. Upper graphs show the contribution to El Niño peaks, and the lower graphs show the contribution to La Niña peaks. The dark and light bars indicate high and low skewness eras, respectively. The ratios of heating terms that are greater or less than critical values, i.e., ±0.5 mon^{-1} for observation and ±0.3 mon^{-1} for models, respectively, are shown at the corners. (g and h) Developing El Niño composite of precipitation anomalies for good and less-skewed models for each 10 percentile (i.e., top 10%, 10%–20%, and 20%–30%). Significant differences at the 95% confidence level are shaded. (i) Difference of maximum precipitation-anomaly longitudes between extreme (top 10%) and moderate (10%–40%) El Niño versus the maximum normalized skewness of the models' Niño3 SSTa. The solid line indicates the regression line, and the "plus" sign indicates the maximum observational value.

El Niño. The asymmetric contribution is defined as the sum of El Niño and La Niña contributions (e.g., Figure 1c and Figures 2b and 2c).

3. Results and Discussion

The observed ENSO is positively skewed, and the present-day observed value (Figure 2a) of normalized skewness (1983–2013; see Methods for details) is +0.9. A positive value means that El Niño grows greater in amplitude than La Niña, usually manifested as more extreme El Niño. We focus on the last push of warming (cooling) into extreme El Niño (La Niña) and pick cases of El Niño (La Niña) developing pitch of the top 10% ENSO. The 31 year running climatology is first removed from the Niño3 SST index, and the developing phases of top (bottom) 10% of the anomalies are selected. We then carry out a heat budget analysis over the top 50 m of the Niño3 region for these ENSO pitches during the high and low skewness eras to unravel the dynamics.

3.1. Observed Extreme El Niño

In the observational reanalysis, several nonlinear dynamic heating terms suppress the growth of El Niño and La Niña during high skewness era (e.g., nonlinear zonal and meridional; Figure 1b), but make only a small contribution to the positive skewness during low skewness era. The nonlinear vertical advection has negative contribution to the skewness in both eras. During the developing stage of El Niño, the vertical component of nonlinear dynamic heating, i.e., $-w'\partial T'_z$, downwells cold anomaly and suppresses the existing anomaly. By contrast, linear advection terms (especially $-u'\partial \overline{T}_x$, $-w'\partial \overline{T}_z$, and $-\overline{v}\partial T'_y$, in terms of the asymmetric contribution (Figure 1c); note that the largest contribution comes from the zonal advection of mean temperature by anomalous currents) significantly promote extreme El Niño during the high skewness era. The linear zonal advective heating is the dominant term that makes the observed extreme El Niño during the high skewness era. These results are different from our previous understanding that extreme El Niño is generated by nonlinear heating, especially vertical advection, and demonstrate the importance of linear advection terms, zonal advection $\left(-u'\partial \overline{T}_x\right)$ in particular, on the generation of extreme El Niño.

As the number of realization of the observation is limited, we deploy state-of-the-art climate models to confirm the importance of the zonal advection of mean temperature revealed in the observation. Although the overall model simulations of the 22 Coupled Model Intercomparison Project Phase 5 (CMIP5) historical runs underestimate the present-day observed skewness (i.e., less extreme El Niño), they show a comparable range of skewness variability on a multi-decadal time scale (Figure 2a). Some models have a normalized skewness that is comparable to the observed, while the others fail—too weak or even negative. To examine the deciding factor of the ENSO asymmetry, we divided models into two groups (good and less-skewed) according to their ability to simulate the observed skewness range.

3.2. Simulated Extreme El Niño

In general, most of the climate models successfully simulate the observed contribution of nonlinear terms; however, averaged across all models, the linear advection terms make little contribution to the simulated asymmetry, and most of the skewness originates from nonlinear terms (Figure 2). The average contribution of linear dynamic heating terms are smaller than those in the observational reanalysis, while the nonlinear dynamic heating terms are comparable to the observed values. Nevertheless, in the good models, the contribution of the linear terms to the asymmetry is considerable (Figure 2b), but the linear terms are substantially underestimated in the less-skewed models (Figure 2c). In the heat budgets of the good models, the largest sources of asymmetry in the linear terms are the zonal advection of mean temperature by anomalous current $(-u'\partial \overline{T}_x)$ and thermocline feedback $(-\overline{w}\partial T'_z)$, followed by Ekman pumping $(-w'\partial \overline{T}_z)$ and meridional advection $(-\overline{v}\partial T'_y)$. In particular, the zonal advection always promotes positive skewness in all good models during the high skewness era, but it is insignificant for less-skewed models.

3.3. Zonal Advection

The zonal advection is a dominant process for extreme El Niño in good models (Figures 3a–3f), as in the observational analysis. The zonal advection during El Niño pitch of high skewness era shows a highly nonnormal distribution, which is different from that during La Niña pitch. The zonal advection shows strong clustering at the extreme positive values ($\geq +0.5 \, \text{mon}^{-1}$ in the observation (42% of El Niño developing pitches) and $\geq +0.3 \, \text{mon}^{-1}$ in the models (25%)) in the high skewness era. On the other hand, it is bounded by smaller values in La Niña developing pitch. Other linear terms do not show such a large difference between the high and the low skewness eras or between El Niño and La Niña developing pitches (Figures S5–S7 in the supporting information), further underscoring the importance of zonal advection. In the observational reanalysis, all other terms (e.g., thermocline feedback) are either small in variance or symmetrically distributed around its mean. The linear zonal advection term is a major source of asymmetry that boosts extreme El Niño, and the same is true for good models when compared between the high and the low skewness eras. The secondary sources of difference in the models are the thermocline feedback (Figures S8–S10 in the supporting information), Ekman pumping, and meridional advection.

3.4. Migration of Atmospheric Response

The generation of the abnormal zonal current that boosts extreme El Niño depends on many factors. Among those factors is the atmospheric variability. The maximum normalized skewness of a model is well correlated with the model's ability to simulate the longitudinal migration of the equatorial precipitation response during extreme El Niño development (Figures 3g–3i). In the observations and good models, the locations of enhanced convection in response to El Niño tend to move from the equatorial western Pacific to the central Pacific, as their intensity gets stronger (Figure 3g); however, those during La Niña do not change much with their strength (Figures S11 and S12 in the supporting information). Only the good models show such a huge migration of the center of action, and the migration is small for the less-skewed models. The linear correlation coefficient between the longitudinal migration and maximum skewness of climate models is over 0.65 (Figure 3i), whose longitudinal migration is defined as the difference in longitudes of the maximum equatorial (5°S–5°N) precipitation anomaly between extreme (top 10% of Niño3 SSTa) and moderate (10%–40%) El Niño. When atmospheric convection moves from the western Pacific to the equatorial central and eastern Pacific where the ocean is more sensitive to atmospheric forcing (Figures S13 and S14 in the supporting information), it excites a stronger zonal current response [*Frauen and Dommenget*, 2010; *Kang and Kug*, 2002; *Su et al*., 2010; *Zhang and Sun*, 2014]. Stronger zonal current boosts developing El Niño anomaly by transporting warm water to the east, enhancing westerly winds, which, in turn, enhance zonal current anomalies. As a result, asymmetric longitudinal eastward migration of convection enhances positive skewness of ENSO. We point out that the historical runs of our good models coincide with the models that exhibit zonal South Pacific Convergence Zone shifts [*Cai et al*., 2012] and models that simulate high rainfall skewness, which show a doubling of extreme El Niño events in the RCP8.5 future simulations [*Cai et al*., 2014].

3.5. Future Implications

Our study provides an insight into future ENSO extremes. With the eastern Pacific warming faster [*Meehl and Washington*, 1996], the Walker circulation is expected to weaken [*Collins et al*., 2010] and move to the east in the warming climate [*Bayr et al*., 2014], which are expected to lead to weaker mean westward currents. This is conducive to atmospheric convection response to El Niño in terms of a shift toward the east (Figure S15 in the supporting information). During the earlier part of the 20th century of the historical runs, the maximum precipitation response occurs around 160°E in response to moderate El Niño SSTa and moves to around 180° during the extreme El Niño. By the end of the 21st century of the RCP8.5 runs, the longitude of maximum precipitation response moves to as far as 160°W during the extreme El Niño. Moreover, although the longitudinal shift is most obvious for top 10% El Niño (higher threshold) in the historical runs, it is seen to occur at the top 20% El Niño intensity (lower threshold) in the future simulation. In association, the zonal current anomaly in these extremes generally strengthens in the future simulation. As the mean westward zonal current weakens (from $-0.13 \pm 0.04 \, \mathrm{m \, s^{-1}}$ to $-0.07 \pm 0.04 \, \mathrm{m \, s^{-1}}$ (ensemble mean ± 1 standard deviation of model spreads)), the net effect of eastward zonal advection [*Santoso et al*., 2013] will become stronger. In the future runs, the frequency of the occurrence of the reversed (eastward) total zonal current increases by 60% compared to that in the historical simulations. This underpins the increasing number of extreme El Niño events in the warming climate as reported by previous studies [*Cai et al*., 2014; *Johnson*, 2014].

4. Conclusion and Further Remarks

We showed that El Niño grows into an extreme event predominantly because of linear advection terms, especially the zonal advection of mean temperature by anomalous zonal currents, which provides the last push to extreme El Niño. The nonlinear advection terms are secondary and serve to suppress the generation of strong La Niña. Most of the CMIP5 models successfully simulate the observed contribution of nonlinear terms. However, they generally underestimate the role of the linear advection terms, meaning most of the asymmetry originates from nonlinear terms instead. Some good models, on the other hand, which are able to produce comparable skewness to the observed value, show that the linear zonal advection term is the major source of its ENSO asymmetry. By contrast, less-skewed models fail to simulate the contribution of the linear terms to the asymmetry. This suggests that current climate models' failure to

adequately reproduce the observed asymmetry of ENSO does not stem from their incapability of simulating nonlinear ocean dynamics.

The abnormal eastward zonal current, which gives the last push to extreme El Niño in the observations, is generally underestimated in the CMIP5 models. While the observed zonal current during extreme El Niño is clearly distinguishable from the normal conditions (i.e., the total current reverses its direction [*Kim and Cai*, 2014; *Santoso et al.*, 2013]), such a feature is not as conspicuous in the model simulations. The anomalous zonal current anomaly is coupled with the extent of an eastward migration of the atmospheric convection center along the equatorial Pacific. In observations, the atmospheric convection moves to the central Pacific, where the ocean is more sensitive to atmospheric forcing, as El Niño gets stronger. Only the good models simulate a significant migration of convection and thus induced anomalous zonal current. The reason for the underestimated skewness of ENSO and the absence of the abnormal current in the less-skewed models is the smaller convective activity over the equatorial central Pacific due to smaller migration of atmospheric response.

In the warming climate, the fast warming in the east is expected to facilitate the eastward movement of the convective response, favoring the generation of anomalous zonal current, and the zonal advection feedback, underpinning the increased frequency of extreme El Niño events.

References

Adler, R. F., et al. (2003), The version-2 Global Precipitation Climatology Project (GPCP) monthly precipitation analysis (1979–present), *J. Hydrometeorol.*, *4*(6), 1147–1167.

An, S.-I., and F.-F. Jin (2004), Nonlinearity and asymmetry of ENSO, *J. Clim.*, *17*(12), 2399–2412.

Bayr, T., D. Dommenget, T. Martin, and S. Power (2014), The eastward shift of the Walker Circulation in response to global warming and its relationship to ENSO variability, *Clim. Dyn.*, *43*(9–10), 2747–2763.

Cai, W., P. van Rensch, T. Cowan, and A. Sullivan (2010), Asymmetry in ENSO teleconnection with regional rainfall, its multidecadal variability, and impact, *J. Clim.*, *23*(18), 4944–4955.

Cai, W., et al. (2012), More extreme swings of the South Pacific convergence zone due to greenhouse warming, *Nature*, *488*(7411), 365–369.

Cai, W., S. Borlace, M. Lengaigne, P. van Rensch, M. Collins, G. Vecchi, A. Timmermann, A. Santoso, M. J. McPhaden, and L. Wu (2014), Increasing frequency of extreme El Niño events due to greenhouse warming, *Nat. Clim. Change*, *4*, 111–116.

Carton, J. A., and B. S. Giese (2008), A reanalysis of ocean climate using Simple Ocean Data Assimilation (SODA), *Mon. Weather Rev.*, *136*(8), 2999–3017.

Collins, M., et al. (2010), The impact of global warming on the tropical Pacific Ocean and El Niño, *Nat. Geosci.*, *3*(6), 391–397.

Duan, W., H. Xu, and M. Mu (2008), Decisive role of nonlinear temperature advection in El Niño and La Niña amplitude asymmetry, *J. Geophys. Res.*, *113*, C01014, doi:10.1029/2006JC003974.

Frauen, C., and D. Dommenget (2010), El Niño and La Niña amplitude asymmetry caused by atmospheric feedbacks, *Geophys. Res. Lett.*, *37*, L18801, doi:10.1029/2010GL044444.

Frauen, C., D. Dommenget, N. Tyrrell, M. Rezny, and S. Wales (2014), Analysis of the non-linearity of El Niño Southern Oscillation teleconnections, *J. Clim.*, *27*, 6225–6244.

Gebbie, G., I. Eisenman, A. Wittenberg, and E. Tziperman (2007), Modulation of westerly wind bursts by sea surface temperature: A semistochastic feedback for ENSO, *J. Atmos. Sci.*, *64*(9), 3281–3295.

Hoerling, M. P., A. Kumar, and M. Zhong (1997), El Niño, La Niña, and the nonlinearity of their teleconnections, *J. Clim.*, *10*(8), 1769–1786.

Jin, F.-F., S.-I. An, A. Timmermann, and J. Zhao (2003), Strong El Niño events and nonlinear dynamical heating, *Geophys. Res. Lett.*, *30*(3), 1120, doi:10.1029/2002GL016356.

Johnson, N. C. (2014), Atmospheric science: A boost in big El Niño, *Nat. Clim. Change*, *4*(2), 90–91.

Kang, I.-S., and J.-S. Kug (2002), El Niño and La Niña sea surface temperature anomalies: Asymmetry characteristics associated with their wind stress anomalies, *J. Geophys. Res.*, *107*(D19), 4372, doi:10.1029/2001JD000393.

Kerr, R. A. (1999), Big El Niños ride the back of slower climate change, *Science*, *283*(5405), 1108–1109.

Kim, W., and W. Cai (2014), The importance of the eastward zonal current for generating extreme El Niño, *Clim. Dyn.*, *42*(11–12), 3005–3014.

McPhaden, M. J. (1999), El Niño: The child prodigy of 1997–98, *Nature*, *398*(6728), 559–562.

Meehl, G. A., and W. M. Washington (1996), El Niño-like climate change in a model with increased atmospheric CO2 concentrations, *Nature*, *382*(6586), 56–60.

Monahan, A. H., and A. Dai (2004), The spatial and temporal structure of ENSO nonlinearity, *J. Clim.*, *17*(15), 3026–3036.

Park, J.-Y., J.-S. Kug, J. Park, S.-W. Yeh, and C. J. Jang (2011), Variability of chlorophyll associated with El Niño–Southern Oscillation and its possible biological feedback in the equatorial Pacific, *J. Geophys. Res.*, *116*, C10001, doi:10.1029/2011JC007056.

Philander, S. G. H. (1983), Anomalous El Niño of 1982–1983, *Nature*, *305*, 16.

Philip, S., and G. J. van Oldenborgh (2009), Significant atmospheric nonlinearities in the ENSO cycle, *J. Clim.*, *22*(14), 4014–4028.

Santoso, A., S. McGregor, F.-F. Jin, W. Cai, M. H. England, S.-I. An, M. J. McPhaden, and E. Guilyardi (2013), Late-twentieth-century emergence of the El Niño propagation asymmetry and future projections, *Nature*, *504*, 126–130.

Smith, T. M., R. W. Reynolds, T. C. Peterson, and J. Lawrimore (2008), Improvements to NOAA's historical merged land-ocean surface temperature analysis (1880–2006), *J. Clim.*, *21*(10), 2283–2296.

Sponberg, K. (1999), *Compendium of Climatological Impacts*, National Oceanic and Atmospheric Administration, Office of Global Programs, Washington, D. C.

Su, J., R. Zhang, T. Li, X. Rong, J.-S. Kug, and C.-C. Hong (2010), Causes of the El Niño and La Niña amplitude asymmetry in the equatorial Eastern Pacific, *J. Clim.*, *23*(3), 605–617.

Taylor, K. E., R. J. Stouffer, and G. A. Meehl (2011), An overview of CMIP5 and the experiment design, *Bull. Am. Meteorol. Soc.*, *93*(4), 485–498.

Timmermann, A., F.-F. Jin, and J. Abshagen (2003), A nonlinear theory for El Niño bursting, *J. Atmos. Sci.*, *60*(1), 152–165.

Yeo, S.-R., and K.-Y. Kim (2014), Global warming, low-frequency variability, and biennial oscillation: An attempt to understand the physical mechanisms driving major ENSO events, *Clim. Dyn.*, *43*(3–4), 771–786.

Zhang, T., and D.-Z. Sun (2014), ENSO asymmetry in CMIP5 models, *J. Clim.*, *27*, 4070–4093.